JOURNAL OF SOLID STATE CHEMISTRY 101, 275–295 (1992)

The Soft Chemical Synthesis of TiO_2 (B) from Layered Titanates

THOMAS P. FEIST* AND PETER K. DAVIES†

Department of Materials Science and Engineering, University of Pennsylvania, Philadelphia, Pennsylvania 19104

Received December 19, 1991; in revised form May 6, 1992; accepted May 7, 1992

Proton exchange and subsequent dehydration of layered titanates with the formula $A_2Ti_nO_{2n+1}$ (A = Na, K, Cs; $3 \leq n \leq 6$) yield TiO_2 (B) at temperatures below 350°C. In order to elucidate the mechanism of TiO_2 (B) formation, we have characterized these reactions using thermal analysis and crystallographic techniques, and we have examined the effect of different starting materials on the formation of TiO_2 (B). The dehydration proceeds through three distinct steps: an initial topotactic structural condensation, which is endothermic, followed by an exothermic nucleation and growth step that results in the formation of a TiO_2 (B)-like intermediate, and a final, low-energy transformation, which yields TiO_2 (B). The structures of $D_2Ti_3O_7$ and TiO_2 (B) have been refined from powder neutron diffraction data in order to better understand the relationship between the initial titanate structures and the formation of TiO_2 (B).

Introduction

Low temperature synthetic techniques can be used to facilitate the formation of metastable structures or thermodynamically stable phases at temperatures well below previous kinetic limitations. Materials made by these routes often demonstrate new or enhanced properties. An example is the preparation of the metastable TiO_2 (B) structure from the layered alkali metal titanate $K_2Ti_4O_9$, first reported by Marchand *et al.* (*1*). Subsequent research by our group (*2, 3*) has shown that TiO_2 (B) can be prepared from several layered titanate precursors. The current work utilizes crystallographic and thermal analysis techniques to study the mechanisms by which various two-dimensional structures transform into the three-dimensional framework of TiO_2 (B) through soft chemical reactions. The ion-exchange properties of the layered materials are presented; the mechanistics of the formation of TiO_2 (B) are discussed; and the relationships between the initial structures and TiO_2 (B) are examined.

Titanates with the formula $A_2Ti_nO_{2n+1}$ form a variety of layered structures for $3 \leq n \leq 6$ with alkali metal (A) cations in the interlayer space. These structures, several of which are presented in Fig. 1, are composed of corrugated ribbons of edge-sharing TiO_6 octahedra. The ribbons are n octahedra wide and join corners to form "stepped" layered structures. (In this paper, we use the terms "step 3," "step 4," and "step 5" to denote structures with, respectively, three, four, or five edge-sharing octahedra

* Current address: Dupont Experimental Station, Wilmington, DE 19880-0262.

† To whom correspondence should be addressed.

0022-4596/92 $5.00

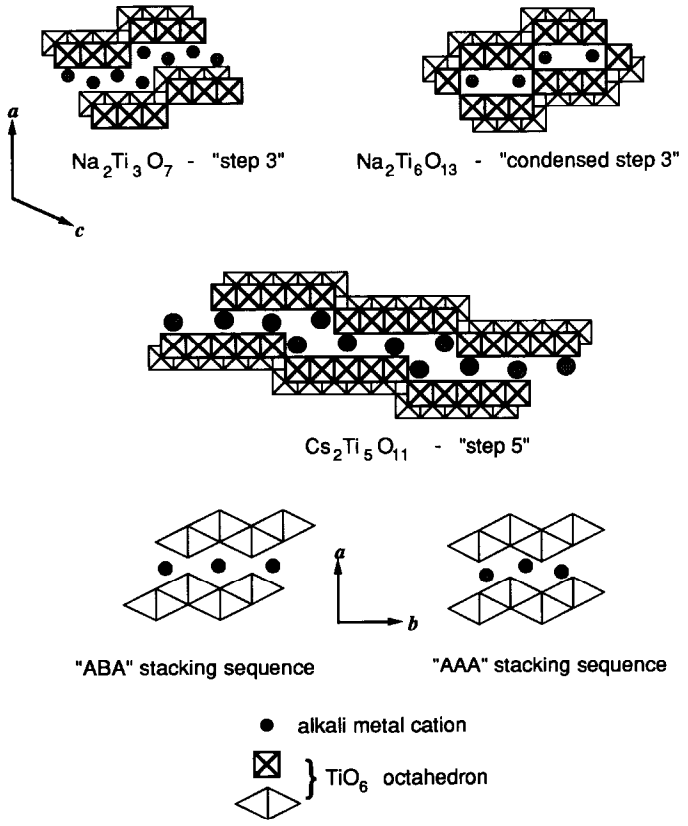

FIG. 1. The structure of layered titanates.

between corner-sharing locations.) The step length for a given composition is determined by the A^+ to Ti^{4+} ratio. The Ti–O layers stack in the *a* direction, with monovalent ions between the layers. In addition to the simple layered structures, tunnel structures can be formed by connecting corners of opposing octahedra to link the layers together. These structures, of which $Na_2Ti_6O_{13}$ is an example, are observed in certain alkali metal systems for $n \geq 6$.

The two-dimensional structure of layered titanates allows for appreciable mobility of the interlayer cations, and ion-exchange properties are observed for a variety of organic and inorganic ions. Dion *et al.* (*4*) demonstrated that $K_2Ti_4O_9$ undergoes quantitative exchange with the alkali metal cations, Tl^+, and Ag^+ through a simple molten salt exchange. Marchand *et al.* (*1*) hydrolyzed a sample of the layered titanate $K_2Ti_4O_9$ in 3 *M* nitric acid, yielding $H_2Ti_4O_9 \cdot H_2O$, which transformed into the three-dimensional framework structure TiO_2 (B) upon heating to 500°C. This novel method of acid exchange followed by gentle heating is as "chimie douce," or soft chemistry, because the reaction proceeds at relatively low temperatures.

The structure of TiO_2 (B), like that of its layered precursor, is composed of corrugated sheets of edge- and corner-sharing TiO_6 octahedra, but the sheets are joined together to form a three-dimensional frame-

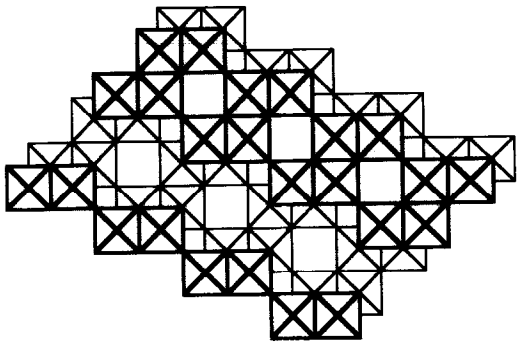

FIG. 2. The structure of TiO_2 (B).

work (Fig. 2). TiO_2 (B) is isotypic with VO_2 (B) (*5*) and has the same framework structure as the sodium titanate bronze Na_xTiO_2 (*6*). Compared to the stable forms of TiO_2, TiO_2 (B) demonstrates enhanced electrochemical and catalytic properties, which have been discussed previously (*7–9*). In addition to addressing the synthesis and properties of TiO_2 (B), Tournoux and co-workers have presented several papers discussing mechanistic aspects of the formation of TiO_2 (B) (*10–13*). The authors observed that the transformation occurs in several distinct steps, though they concluded that no stable intermediates existed among the layered titanate structure, $H_2Ti_4O_9$, and TiO_2 (B). They also suggested that the reaction is topotactic, without supplying a specific reaction mechanism, and that the formation of TiO_2 (B) was dependent on the starting titanate structure.

Izawa *et al.* (*14*) examined acid exchange and dehydration of the step 3 titanate $Na_2Ti_3O_7$, which they reported formed only anatase upon dehydration, and of the step 4 potassium structure. The workers presented a topotactic mechanism in which $H_2Ti_4O_9$ condenses to form the tunnel structure $H_2Ti_8O_{17}$, which then shears to form TiO_2 (B). Marchand *et al.* (*10*) sharply criticized this theory of TiO_2 (B) formation, demonstrating several severe inconsistencies in the interpretation of X-ray diffraction data, and subsequent work by our group (*3*) revealed that X-ray diffraction data presented for $H_2Ti_3O_7$ also had been incorrectly and incompletely indexed. Izawa *et al.* had concluded that the AAA stacking sequence of layers in the step 3 compound (Fig. 1) prevents the structural condensation they suggested for the step 4 material.

Mocarski (*2*) examined the ion-exchange/dehydration behavior of the step 5 titanate $Cs_2Ti_5O_{11}$, the infinite layer structure $Cs_2Ti_6O_{13}$, and the condensed tunnel structure $Na_2Ti_6O_{13}$. He showed that TiO_2 (B) is formed upon dehydration of the stepped and tunnel structures and that TiO_2 (rutile) and TiO_2 (B) are the final products of the infinite layer structure.

The original work on TiO_2 (B) (*13*) suggested that the entire transformation from layered titanate to TiO_2 (B) was dependent on the starting titanate structure—specifically a step 4 structure. The workers suggested that each step of the reaction was topotactic, and one can imagine this being true for the step 4 compound. Since the structure contains ribbons of four octahedra, each unit could be split, or sheared, to form the double octahedral blocks that compose TiO_2 (B). There is not, however, an equivalent topotactic route to the formation of TiO_2 (B) from layered compounds which contain an odd number of octahedra in each step. Therefore, if the proposed mechanism is applied to step 3 or step 5 titanates, one might expect that these starting materials would yield other new forms of TiO_2 upon ion exchange and dehydration. This is not the case, though, and all of the titanates yield TiO_2 (B).

The current work examines the transformations of various layered materials into TiO_2 (B) by investigating the relationships among the structures of different starting structures, TiO_2 (B), and intermediates observed during its synthesis. The investiga-

tion centers on the step 3 titanate $Na_2Ti_3O_7$, which had not previously been shown to form TiO_2 (B) upon ion exchange and dehydration.

Experimental Procedure

Alkali metal titanates, $A_2Ti_nO_{2n+1}$ ($n = 3$, $A = Na$; $n = 4$, $A = K$; $n = 5$, $A = Cs$) were prepared by conventional solid state methods. Stoichiometric quantities of dried alkali metal carbonate (Na_2CO_3, K_2CO_3) or nitrate ($CsNO_3$) and TiO_2 (anatase) were ground under acetone by mortar and pestle, isostatically pressed at ~50,000 psi to form a pellet, and fired overnight in a Pt crucible in air at 850°C. The sintered pellet was pulverized, and the procedure was repeated once. The products were analyzed by powder X-ray diffraction (XRD).

Acid exchange of the layered titanates was achieved below 100°C in aqueous solution. The powdered alkali metal titanate was immersed in a 200-fold excess (by weight) of 1 *M* HCl and stirred at 60°C for 1 day ($Cs_2Ti_5O_{11}$) or 3 days ($Na_2Ti_3O_7$ and $K_2Ti_4O_9$). The resulting products were retrieved by vacuum filtration, washed with deionized water, and dried in air.

Powder XRD was used to examine the structure of all exchanged materials; atomic absorption (AA) and inductively coupled plasma (ICP) spectroscopies were used to verify sample composition; and thermogravimetric analysis (TGA) was used to examine weight loss behavior. Scanning electron microscopy (Philips SEM 500) was used to characterize particle size and morphology.

Acid exchange of the tunnel structure $Na_2Ti_6O_{13}$ was achieved by immersing a 1-g sample of material in molten NH_4NO_3 contained in a fused silica tube for several days at 200°C in a vertical tube furnace. After allowing the sample to cool, the ammonium nitrate was dissolved in deionized water, the remaining titanate was recovered by vacuum filtration, and the sample was dried in air. More complete exchange was achieved by repeating the process. A combined TGA/mass spectroscopy system was used to monitor species liberated during thermal treatment of the material, and the pH of evolved gas passing through a water bubbler was monitored during TGA measurements.

TGA traces for all layered titanates showed multistep weight loss behavior, indicating potential formation of discrete structural intermediates during the dehydration reaction. Two approaches were used to isolate and characterize these intermediate structures: high temperature, *in situ* XRD and powder diffraction measurements on samples quenched from high temperature.

The energetics of structural transformations observed during the formation of TiO_2 (B) were measured by differential scanning calorimetry (DSC) using a Setaram DSC111 with automated data acquisition and baseline subtraction. Measurements were made under static air at a heating rate of 5°/min.

Transmission electron microscopy (TEM) was used primarily to gather electron diffraction data from intermediates observed during the formation of TiO_2 (B). A Philips 400T was used to collect diffraction data and lattice images on specimens that were prepared by grinding under acetone followed by dispersion onto a holey carbon film supported on a copper grid.

Powder neutron diffraction proved to be a very useful technique for investigating acid-exchanged layered titanates and TiO_2 (B). Deuterium was substituted for H^+ in the layered structures, and its position was investigated directly using neutron diffraction. Deuterium exchange of layered titanates was similar to the typical acid-exchange reactions, with two exceptions: deuterated solvents (DCl and D_2O) were used, and the entire procedure was performed in a helium-filled glovebag to avoid hydrogen exchange

between the deuterated materials and the atmosphere.

Neutron diffraction data were collected at the High Flux Beam Reactor (HFBR) at Brookhaven National Laboratory and at the research reactor of Atomic Energy of Canada Limited (AECL). At the HFBR, data were collected using a Si(220) incident beam monochromator (λ = 1.338 Å). Samples were contained in thin-walled aluminum sample cans which were placed in a second, outer can sealed with an indium gasket to prevent atmospheric interactions. Data were collected at room temperature from 5° to 120° 2θ in 0.05° or 0.1° steps. At AECL, a Si(115) incident beam monochromator was used (λ = 1.4988 Å). The samples were contained in vanadium sample cans, sealed with an indium gasket, and placed in an evacuated Displex, allowing sample temperatures between 15 K and ambient temperature during data collection. Data were collected to 120° 2θ in steps of 0.05°.

Results

The solid state synthetic route described above produced single-phase white powders with powder XRD patterns that compared closely to those reported in the literature for the appropriate alkali metal titanate: $Na_2Ti_3O_7$ (*15*), $Na_2Ti_6O_{13}$ (*16*), $K_2Ti_4O_9$ (*4*), or $Cs_2Ti_5O_{11}$ (*17*). Scanning and transmission electron microscopy show $Na_2Ti_3O_7$ particles to have a platey or lathlike habit. Each of the other materials has the fibrous morphology reported previously.

Complete exchange of Na^+ by H^+ in $Na_2Ti_3O_7$ was achieved by stirring the starting layered titanate in a 200-fold excess of 1 *M* HCl for 3 days, as reported by Izawa *et al.* (*14*). Figure 3 shows TGA data for the dehydration of exchanged $Na_2Ti_3O_7$. The total weight loss corresponds to 1 mole of H_2O compared to the final product $3TiO_2$, giving an initial composition of $H_2Ti_3O_7$. Elemental analysis confirmed that the residual Na

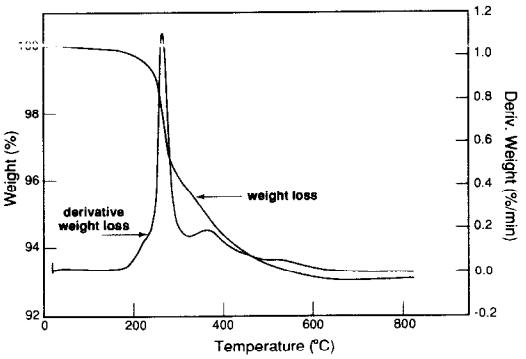

FIG. 3. TGA of acid-exchanged $Na_2Ti_3O_7$.

content was less than 0.25 wt%, which corresponds to $Na_{0.03}H_{1.97}Ti_3O_7$. More complete exchange can be achieved by repeating the exchange process with a fresh acid solution. Particle size had no discernible effect on the formation of TiO_2 (B) from $H_2Ti_3O_7$.

The powder XRD data for $H_2Ti_3O_7$ are shown in Table I, and the pattern of $H_2Ti_3O_7$ shows no residual $Na_2Ti_3O_7$. The data agree with that reported by Izawa *et al.* (*14*), but interpretation of the data differs significantly and is addressed under Discussion. The diffraction peaks are shifted considerably from those of $Na_2Ti_3O_7$, and an indexing scheme analogous to that for $Na_2Ti_3O_7$ does not account for all the observed peaks. The lattice parameters of $Na_2Ti_3O_7$ (space group $P2_1/m$) are a = 8.57 Å, b = 3.80 Å, c = 9.14 Å, and β = 101.57°, but the present data were indexed to a new monoclinic cell with the indices in Table I. The refined lattice parameters for $H_2Ti_3O_7$ are a = 16.03 Å, b = 3.75 Å, c = 9.19 Å, and β = 101.45°. The observed extinctions indicate a *C*-centered cell, implying a space group of *Cm*, *C*2, or *C*2/*m*.

SEM and TEM demonstrate a needlelike, fibrous morphology for the acid-exchanged material, with an average particle length of 1 to 5 μm and a width less than or equal to 0.5 μm. TEM and electron diffraction show

TABLE I

X-RAY POWDER DIFFRACTION DATA FOR $H_2Ti_3O_7$

h	k	l	d_{calc} (Å)	d_{obs} (Å)	I_{obs}
0	0	1	9.01	9.01	7
2	0	0	7.86	7.87	100
2	0	−1	6.61	6.61	4
2	0	1	5.42	5.41	48
0	0	2	4.51	4.51	7
2	0	−2	4.30	4.29	1
4	0	0	3.93	3.93	3
1	1	0	3.65	3.65	25
2	0	2	3.61	3.61	10
1	1	−1	3.44	3.43	2
4	0	1	3.37	3.37	4
4	0	−2	3.31	3.31	3
3	1	0	3.05	3.05	7
0	0	3	3.00	3.00	40
3	1	1	2.79	2.79	5
3	1	−2	2.67	2.67	3
2	0	3	2.64	2.64	9
6	0	−2	2.49	2.49	19
6	0	1	2.39	2.39	4
1	1	−3	2.37	2.37	4
5	1	−2	2.27	2.27	2
1	1	3			
0	0	4	2.25	2.25	4
6	0	−3	2.20	2.20	3
2	0	4	2.06	2.06	24
1	1	−4	1.95	1.95	8
7	1	−1			
8	0	−2	1.88	1.88	
1	1	4			11
0	2	0			

Note. $a = 16.03 \pm 0.002$ Å, $b = 3.75 \pm 0.001$ Å, $c = 9.19 \pm 0.001$ Å, $\beta = 101.45° \pm 0.01°$.

that crystallites generally are elongated along b and tend to lie on the b axis.

The powder XRD pattern of $D_2Ti_3O_7$ was identical to that of $H_2Ti_3O_7$. Elemental analysis confirms that residual sodium was 0.25 wt%, and TGA confirmed nearly complete exchange of D^+ for Na^+. The powder neutron diffraction data for $D_2Ti_3O_7$ were collected at 15 K to minimize the motion of D^+ in the layered structure. Refinement of the neutron diffraction data then proceeded in several steps. Because the positions of D^+ ions in the layered structure were not known initially, but the positions of framework ions could be well postulated from the XRD data, the Ti–O framework alone was first refined to a minimum value of $R_{wp} = 0.061$. The raw neutron diffraction data, final calculated pattern, and difference profile for the Ti_3O_7 framework are presented in Fig. 4, and the final refined parameters are shown in Table II. A difference Fourier map was then generated from the observed and calculated structure factors. The results of the difference Fourier, bond lengths angles from the framework, and literature data for similar protonated systems were used to place D^+ in appropriate positions between the layers, and the refinement continued. These results are addressed in depth in the discussion section.

Complete exchange of H^+ for Cs^+ was achieved by stirring $Cs_2Ti_5O_{11}$ in a 200-fold excess of 1 *M* HCl for 24 hr, as reported by Mocarski (*2*). Elemental analysis by ICP shows residual Cs to be less than 2 wt%, which is equivalent to the composition $Cs_{0.06}H_{1.94}Ti_5O_{11}$. Figure 5 shows TGA data for the dehydration of exchanged $Cs_2Ti_5O_{11}$. (The TGA of acid-exchanged $K_2Ti_4O_9$ is shown in Fig. 6 for comparison.) The total weight loss corresponds to 3.5 mol of H_2O compared to the final product $5TiO_2$, giving an initial composition of $H_2Ti_5O_{11} \cdot 2.5H_2O$. XRD confirms that the starting layered structure is maintained during the exchange reaction.

Proton exchange of $Na_2Ti_6O_{13}$ was achieved by treatment of the starting material in molten NH_4NO_3 for 3 days. The species exchanged for Na^+ is not NH_4^+, as might be expected, but H^+. Monitoring the gases evolved during heating the exchanged material showed that there is no evolution of ammonia or nitrogen during the weight loss, only H_2O, indicating that only H^+ replaced Na^+ in the structure. Although ammonium ions are readily exchanged in layered titanates, the channel size is restricted in $Na_2Ti_6O_{13}$ because the layers are joined

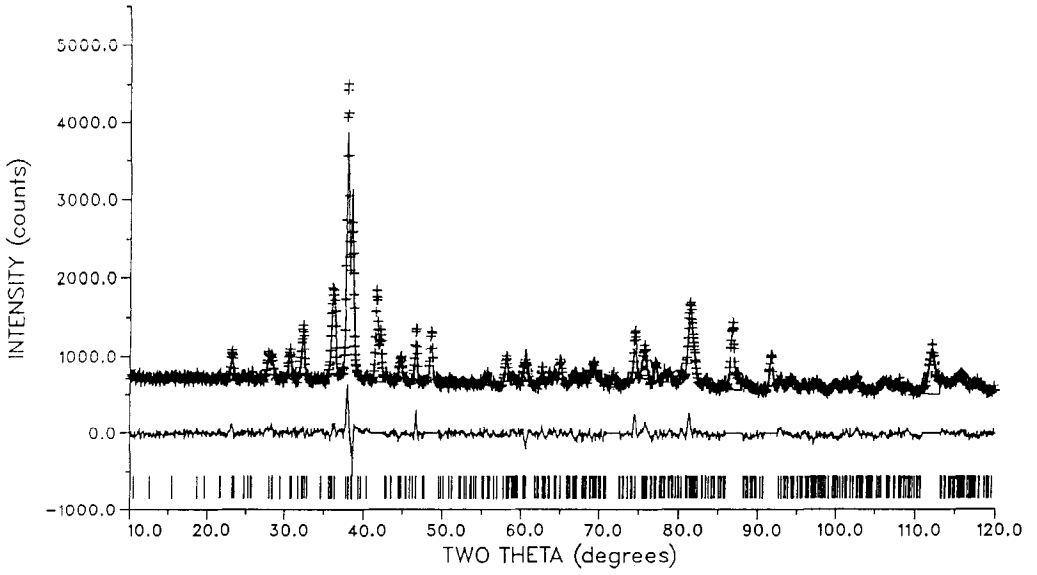

FIG. 4. Final observed (+) and calculated (solid line) neutron diffraction patterns for the Ti_3O_7 framework of $D_2Ti_3O_7$. Excluded regions correspond to peaks from the Cu temperature probe.

though corner-shared oxygen atoms (Fig. 1). Therefore, it is not surprising that the large ammonium ion is not exchanged, and only H^+ is inserted during the exchange reaction. Multiple molten salt treatments were necessary to achieve complete exchange of H^+ for Na^+, and nearly complete exchange was attained after three successive ammonium nitrate treatments.

Thermogravimetry for each of the layered systems shows multistep weight loss behavior, which is especially evident when examining the derivative weight loss curves (Figs. 3, 5, and 6). The weight losses are tabulated

TABLE II

FINAL ATOMIC PARAMETERS FROM THE RIETVELD REFINEMENT OF THE Ti–O FRAMEWORK OF $D_2Ti_3O_7$

Atom	x	z	B (Å^2)	Occupancy
Ti(1)	0.225 (002)	0.223 (004)	0.2	1
Ti(2)	0.168 (002)	0.511 (004)	0.2	1
Ti(3)	0.125 (002)	0.823 (003)	0.2	1
O(1)	0.169 (001)	0.041 (002)	0.5	1
O(2)	0.134 (001)	0.316 (002)	0.5	1
O(3)	0.085 (001)	0.608 (003)	0.5	1
O(4)	0.007 (001)	0.855 (002)	0.5	1
O(5)	0.349 (001)	0.176 (002)	0.5	1
O(6)	0.290 (001)	0.462 (002)	0.5	1
O(7)	0.239 (001)	0.744 (003)	0.5	1

Note. $a = 16.025 \pm 0.003$ Å, $b = 3.747 \pm 0.001$ Å, $c = 9.188 \pm 0.001$ Å, $\beta = 101.457° \pm 0.010°$. $R_{exp} = 0.037$, $R_p = 0.047$, $R_{wp} = 0.061$, $R_B = 0.162$.

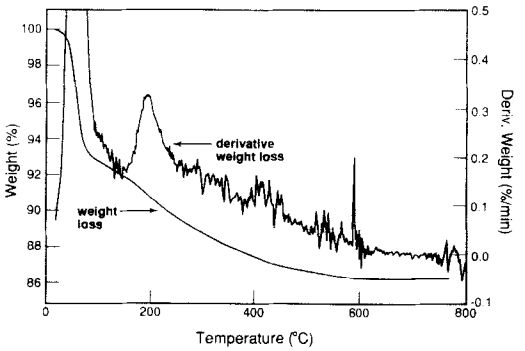

FIG. 5. TGA of acid-exchanged $Cs_2Ti_5O_{11}$.

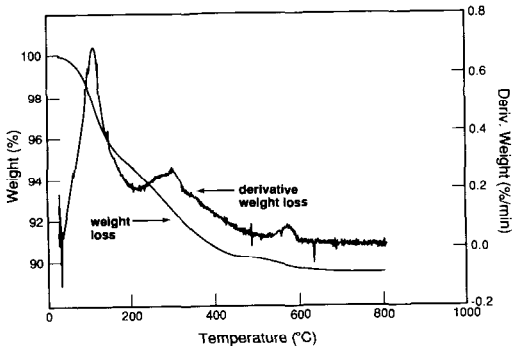

FIG. 6. TGA of acid-exchanged $K_2Ti_4O_9$.

in Table III. The powder XRD pattern of the final product of each dehydration reaction is identical to that of TiO_2 (B) as reported by Marchand *et al.* (*1*). X-ray diffraction indicates that all samples contain a small amount of anatase, with TiO_2 (B) prepared from $Cs_2Ti_5O_{11}$ showing the greatest amount of anatase formed.

TABLE III

SUMMARY OF TGA DATA FOR ACID-EXCHANGED LAYERED TITANATES

	Weight loss (%)	Mole H_2O/ mole titanate
$H_2Ti_3O_7$		
	3.5	0.5
	1.75	0.25
	1.75	0.25
	7.0	1.0
$H_2Ti_4O_9 \cdot H_2O$		
	5.0	1.0
	2.5	0.5
	2.5	0.5
	10.0	2.0
$H_2Ti_5O_{11} \cdot 2.5H_2O$		
	7.8	2.0
	2.0	0.5
	3.9	1.0
	13.7	3.5
$H_2Ti_6O_{13}$		
	3.6	1.0

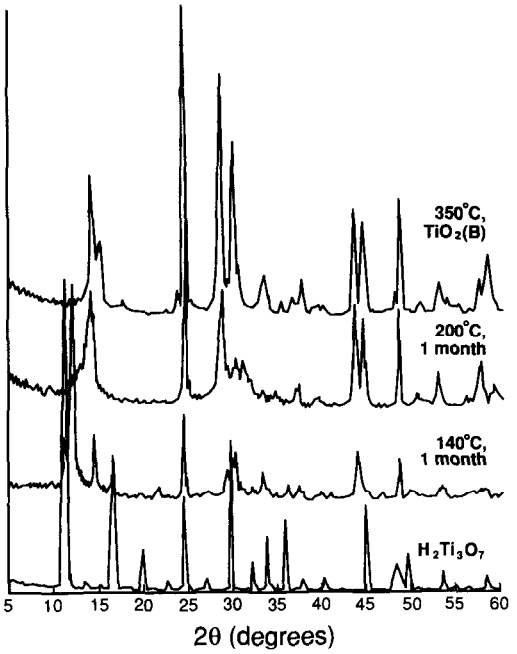

FIG. 7. Powder X-ray diffraction patterns of the dehydration products of acid-exchanged $Na_2Ti_3O_7$.

During the dehydration of $H_2Ti_3O_7$ to TiO_2 (B), two distinct structural intermediates were isolated. Samples removed from the TGA during weight loss steps and samples investigated by *in situ* high temperature XRD were generally multiphase and less crystalline than samples prepared by long-term annealing followed by quenching to ambient temperature. Therefore, the latter method was used to prepare intermediate structures. Figure 7 shows diffraction patterns for intermediates prepared from $H_2Ti_3O_7$ under the conditions indicated. Heating at temperatures between those shown in Fig. 7 produced multiphase materials consisting of the structures observed above and below the temperature. Heating above 350°C produced more crystalline TiO_2 (B), but the amount of anatase formed also increased with temperature.

The ion-exchange product of $Cs_2Ti_5O_{11}$

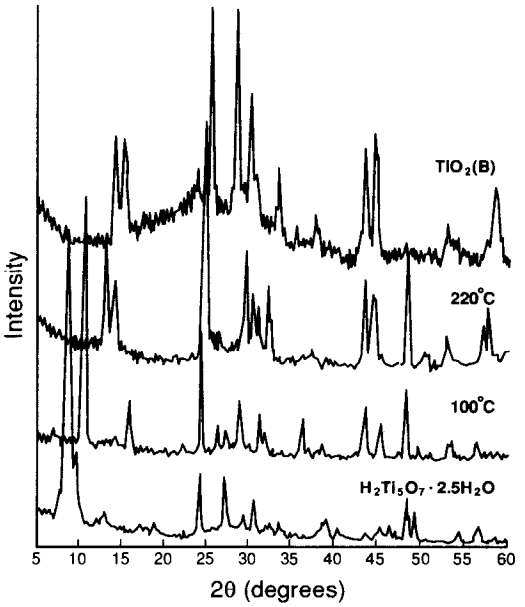

FIG. 8. Powder X-ray diffraction patterns of the dehydration products of acid-exchanged $Cs_2Ti_5O_{11}$.

showed more complicated dehydration behavior than the step 3 materials. Intermediate structures formed during the transformations which lead to TiO_2 (B) are less stable (and hence less crystalline) and proved more difficult to isolate. Figure 8 shows XRD patterns of samples removed from a furnace during dehydration of $H_2Ti_5O_{11} \cdot 2.5H_2O$.

Raman spectroscopy revealed an interesting correlation between the formation of TiO_2 (B) and the step length of the initial layered titanate from which it was formed. As Fig. 9 indicates, the Raman peaks for TiO_2 (B) become increasingly broad as longer step length titanates are used as starting materials. This indicates that the crystallinity of TiO_2 (B) prepared from layered titanates decreases with increasing initial step length.

DSC scans for each of the acid-exchanged layered titanates are shown in Figs. 10–12. Exchanged $K_2Ti_4O_9$ and $Cs_2Ti_5O_{11}$ show large endothermic peaks centered at approximately 100°C. Each titanate shows an endothermic heat effect between 200 and 300°C succeeded by exothermic transitions in the later steps of TiO_2 (B) formation. Figure 13 shows the calorimetry data for the exchanged tunnel structure $H_2Ti_6O_{13}$, which demonstrates a large exotherm below 400°C, but no endothermic low temperature transition. The transitions observed for starting materials with longer step lengths are generally broader and more complicated than those of the step 3 titanates.

The crystal structure of TiO_2 (B) was refined from powder neutron diffraction data collected at AECL at 290 K. The initial fractional atomic positions used were those cal-

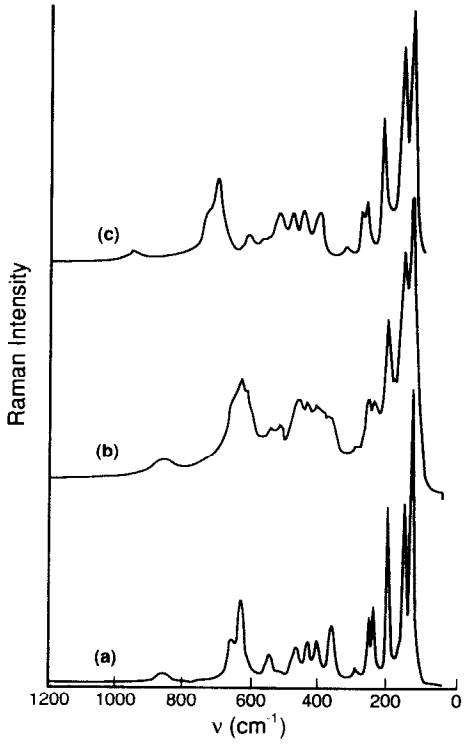

FIG. 9. Raman spectra of TiO_2 (B) prepared from (a) $H_2Ti_3O_7$, (b) $H_2Ti_5O_{11} \cdot 5H_2O$, and (c) $H_2Ti_4O_9 \cdot H_2O$. Frequency scale for c is slightly displaced from that of a and b, but peak positions are independent of starting material.

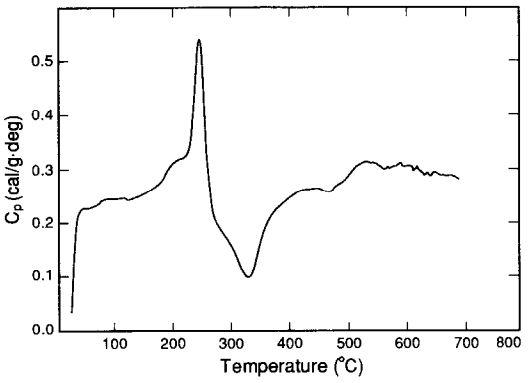

FIG. 10. DSC of acid-exchanged $Na_2Ti_3O_7$.

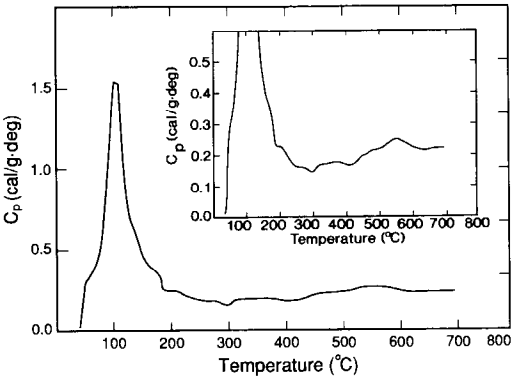

FIG. 12. DSC of acid-exchanged $Cs_2Ti_5O_{11}$.

culated by Catlow *et al.* (*18*) using the energy minimization technique. Refinement of TiO_2 (B) as the only phase present led to a final $R_{wp} = 0.069$ ($R_{exp} = 0.024$), with obvious unaccounted for intensity in several portions of the profile. These unexplained peaks corresponded to the most intense reflections for anatase, so anatase was included as a second phase in the refinement. This inclusion improved the fit considerably, and the refinement proceeded to a final $R_{wp} = 0.043$. The observed data, final calculated pattern, and difference for the profile are presented in Fig. 14, and the refined lattice and atomic parameters are shown in Table IV.

Discussion

The acid-exchange product of $Na_2Ti_3O_7$ ($H_2Ti_3O_7$) has a powder XRD pattern which compares closely to that reported by Izawa *et al.* (*14*), but our interpretation is significantly different. The authors reported a single strong peak at 3.65 Å, to which they assigned a Miller index of (102). They also reported an unindexed peak at $d = 2.374$ Å and did not report several peaks observed in the present work. Izawa *et al.* indexed

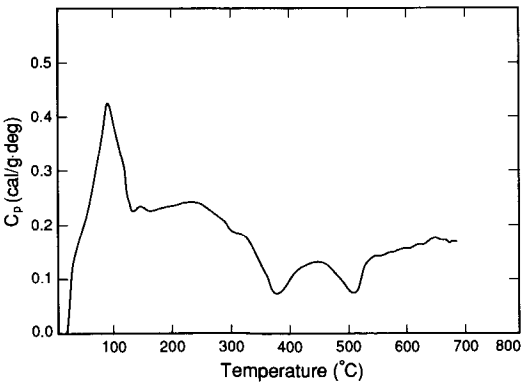

FIG. 11. DSC of acid-exchanged $K_2Ti_4O_9$.

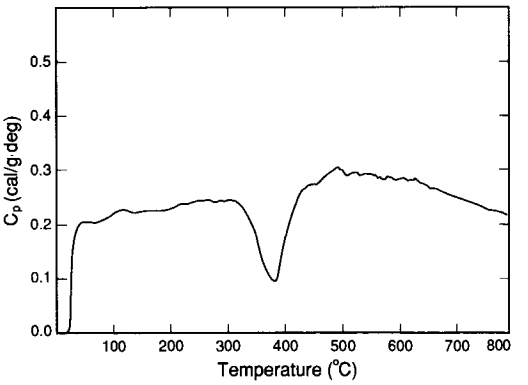

FIG. 13. DSC of acid-exchanged $Na_2Ti_6O_{13}$.

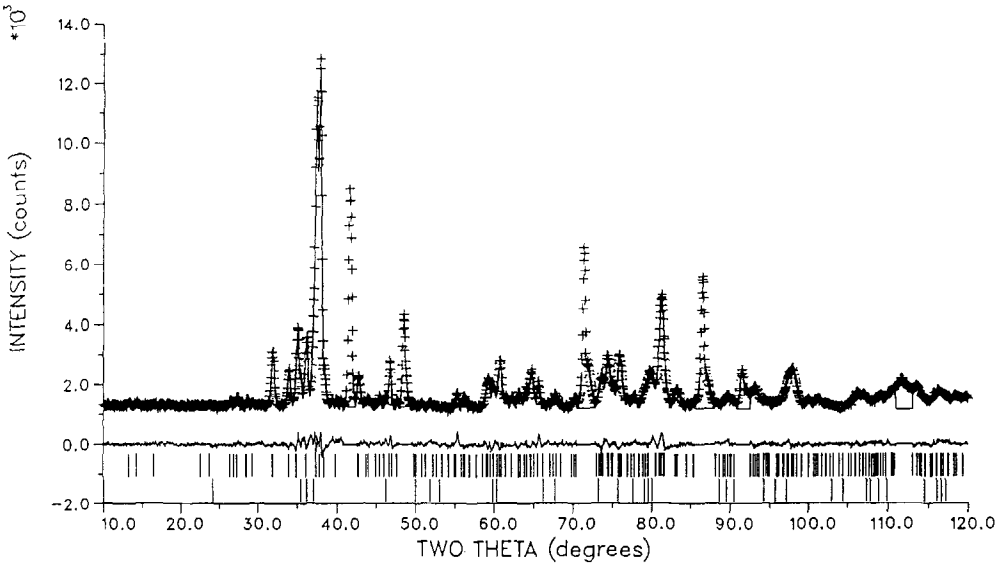

FIG. 14. Final observed (+) and calculated (solid line) neutron difraction patterns for TiO_2 (B). Peak markers are the TiO_2 (B) above anatase. Excluded regions correspond to peaks from the Cu temperature probe.

their data using the same unit cell as $Na_2Ti_3O_7$, which has the space group $P2_1/m$. The structure of $Na_2Ti_3O_7$ differs from that of the other layered titanates by a relative displacement of the layers by $b/2$. In other words, the stacking sequence of layers in $Na_2Ti_3O_7$ is AAA, in contrast to the other titanates which stack in an ABA fashion. The difference, represented in Fig. 1, is possible because the layers are corrugated along the b direction, not stepped as along a. In this work, two peaks, at d = 3.65 and 3.61 Å, were resolved where the previous workers reported only one. Indexing these as the (110) and (202), respectively, yields a unit cell which is consistent with all the observed diffraction data. The new cell, which is C-centered, results from a shift to an ABA arrangement of the layers from the AAA stacking sequence and is consistent with the other acid-exchanged titanates, which stack in an ABA manner. The structural change reflects the increased stability of the new structure, caused by hydrogen bonding between the layers, and is addressed in more detail in the discussion of the neutron diffraction data below.

TABLE IV

FINAL ATOMIC PARAMETERS FROM RIETVELD REFINEMENT OF TiO_2 (B)

Atom	x	z	B (Å^2)	Occupancy
Ti(1)	0.197 (007)	0.292 (011)	0.85 (15)	1
Ti(2)	0.099 (007)	0.705 (012)	0.35 (11)	1
O(1)	0.132 (003)	0.004 (007)	0.10 (07)	1
O(2)	0.264 (004)	0.653 (008)	0.03 (10)	1
O(3)	0.060 (004)	0.371 (006)	0.54 (09)	1
O(4)	0.362 (004)	0.293 (007)	0.87 (12)	1

Note. Data collected at 290 K. a = 12.1787 ± 0.0010 Å, b = 3.7412 ± 0.0002 Å, c = 6.5249 ± 0.0005 Å, β = 107.054° ± 0.004°. R_{exp} = 0.024, R_p = 0.032, R_{wp} = 0.043, R_B = 0.046.

The ABA model was used as a starting point for the full structure refinement of $D_2Ti_3O_7$ from the neutron diffraction data. Unfortunately, the "phase problem" introduced by not including D^+ in the refinement

TABLE V

INTERATOMIC DISTANCES (Å) FOR THE Ti–O FRAMEWORK OF $D_2Ti_3O_7$

Ti(1)		O(2)	
–O(1)	1.789(1)	–O(3)	2.789(1)
–O(2)	1.854(1)	–O(4)	2.529(28)
–O(5)	2.133(1)	–O(6)	2.566(1)
–O(6)	2.243(1)	–O(6)	2.804(18)
–O(7) (2x)	1.965(8)	–O(7)	2.950(1)
Ti(2)		O(3)	
–O(2)	1.707(1)	–O(3)	2.891(20)
–O(3)	1.765(1)	–O(4)	2.930(1)
–O(6)	2.029(1)	–O(5)	2.862(17)
–O(6) (2x)	1.965(8)	–O(6)	2.886(4)
–O(7)	2.267(1)	–O(7)	2.621(1)
Ti(3)		O(4)	
–O(1)	1.959(1)	–O(4)	2.622(1)
–O(3)	2.031(1)		
–O(4)	1.949(1)	O(5)	
–O(5) (2x)	1.934(5)	–O(6)	2.970(1)
–O(7)	2.102(1)	–O(7)	2.507(1)
O(1)		O(6)	
–O(2)	2.811(1)	–O(6)	2.459(1)
–O(4)	2.773(1)	–O(7)	2.956(1)
–O(5)	2.938(1)	–O(7)	2.700(10)
–O(5)	2.664(7)		
–O(7)	2.898(20)		

Note. The estimated standard deviations are in 0.001 Å.

prevented an accurate refinement of the $Ti_3O_7^{2-}$ sheets. The original intention of refining the atomic positions, lattice parameters, and peak shape parameters to a minimum R_{wp} followed by generating a difference Fourier map to locate the deuteriums did not produce a definitive solution. Some progress was made, however, using this approach. Table V shows the interatomic distances obtained from refining the framework ions only. As the table indicates, the O(2)–O(4) interlayer distance is 2.53 Å, and the O(4)–O(4) distance is 2.62 Å, both of which are appropriate separations for hydrogen-bonded oxygens (Fig. 15). The O(3)–O(3) distance of 2.85 Å, which is larger than the other interlayer oxygen distances, is greater than the distance commonly associated with strong hydrogen bonding between two oxygen atoms. The difference Fourier, though obfuscated by the phase problem, showed definite scattering intensity between O(2) and O(4), centered approximately 1 Å from O(4) and 1.5 Å from O(2). The map also showed intensity, which is somewhat weaker, between adjacent O(4)'s. The O(4) atoms are the only oxygens in the structure that are bound to only one titanium, making them the most susceptible to hydrogen bonding. Both of these observations are consistent with hydrogen being strongly bound to the O(4) atom.

The above observation of hydrogen bound to the O(4) is consistent with chemical arguments and with work that has appeared in the literature. Since the O(4) is not shared between Ti atoms, it is more basic than the other (shared) oxygens, and it would logically be most strongly protonated. Rebbah *et al.* (*19*) refined the structure of the acid-exchanged materials $HTiNbO_5$ and $DTiNbO_5$, which are closely related to $D_2Ti_3O_7$ and also demonstrate strong hydrogen bonding between the oxide layers. In those compounds, the proton is located between the corner (unshared) oxygen and the (shared) oxygen across the channel. The two oxygens are separated by 2.5–2.6 Å, and the O–H · · · O bond angle is 180°. As discussed above, the same relationships are observed between O(2) and O(4) in the current material. There is a significant difference between the two structures though: $HTiNbO_5$ contains only one hydrogen per unshared oxygen, but the stoichiometry of $D_2Ti_3O_7$ requires a second type of hydrogen coordination in the structure. That second hydrogen, the position of which is not known exactly, is likely distributed across several sites throughout the structure, including near the O(3) and between the O(4)'s. There is no evidence of hydrogen bonding between the O(3)'s, but the O(4)–O(4) distance is ~2.6 Å, an appropriate distance for hydrogen bonding.

Although the Rietveld refinement does

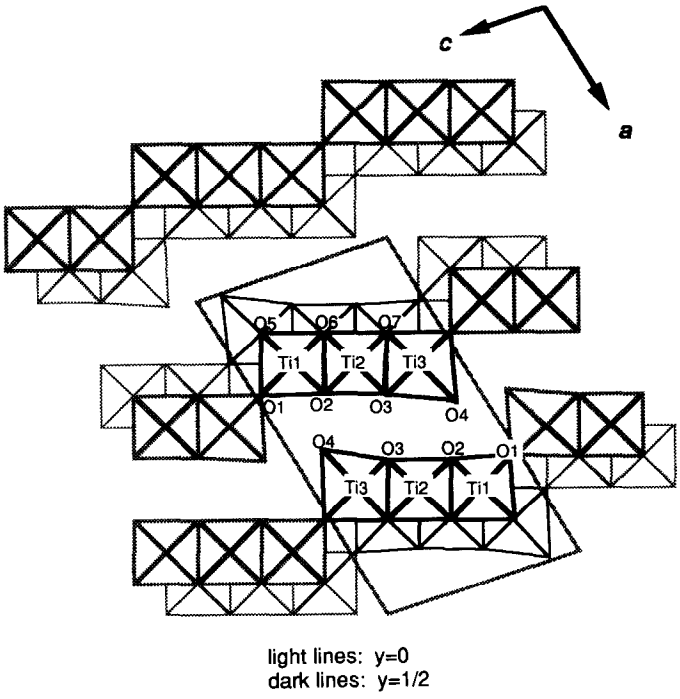

FIG. 15. The framework structure of $D_2Ti_3O_7$.

not provide an ultimate solution to the structure of $D_2Ti_3O_7$, it clearly demonstrates an ABA sequence which is consistent with the stacking observed for exchanged $Cs_2Ti_5O_{11}$ and $K_2Ti_4O_9$. This arrangement of layers provides appropriate oxygen separations for hydrogen bonding between the sheets, which makes the new structure more stable than the AAA precursor. As is shown below, the ABA layer stacking is prerequisite for the formation of TiO_2 (B) from layered titanates.

Each of the acid-exchanged layered titanates undergoes multistep dehydration which leads to the formation of TiO_2 (B). Because the key to describing how TiO_2 (B) forms from these different starting materials lies in understanding each of the dehydration stages, this section compares and contrasts the reactions for the various starting materials.

Heating $H_2Ti_3O_7$ at 140°C for 1 month removed 1 mole of H_2O per 2 mole of sample, yielding $H_2Ti_6O_{13}$ by the reaction:

$$2H_2Ti_3O_7 \rightarrow H_2Ti_6O_{13} + H_2O \uparrow .$$

The X-ray diffraction pattern for this material compares closely to that of $H_2Ti_6O_{13}$ prepared by ion exchange of the condensed step 3 titanate $Na_2Ti_6O_{13}$. The ensuing weight loss behavior of this intermediate structure is identical to that of $H_2Ti_6O_{13}$ prepared by ion exchange of $Na_2Ti_6O_{13}$, and both result in the formation of TiO_2 (B). The logical conclusion from these results is that the first dehydration step during the formation of TiO_2 (B) is a simple topotactic condensation of the layered material, yielding the tunnel structure $H_2Ti_6O_{13}$ (Fig. 1). The conversion of the layered structure from an AAA to ABA stacking sequence during ion exchange is consistent with this transforma-

tion, because the condensed structure has the ABA sequence of layers joined by corner-sharing TiO_6 octahedra.

The next dehydration step for $H_2Ti_3O_7$, which corresponds to the loss of slightly less than 0.25 mole of H_2O compared to the starting material (i.e., $HTi_3O_{6.5} \rightarrow H_{0.5}Ti_3O_{6.25}$), is accompanied by more significant structural rearrangement. Heating for several days at 225°C results in the loss of the step 3 nature of the material and the formation of a structure that XRD shows to be closely related to TiO_2 (B). The material is poorly crystallized, showing broad X-ray diffraction peaks of low intensity. The same structure can be prepared from a sample of $H_2Ti_3O_7$ that had been partially re-exchanged with Na^+ to a composition of $Na_{0.8}H_{1.2}Ti_3O_7$. Heating the material at 800°C in air or He induced the formation of $Na_{0.8}Ti_3O_{6.4}$, just as heating the completely hydrogenated material at 225°C led to $H_xTi_3O_{6.25}$ ($x \approx 0.5$). The Na-containing material, because it was prepared at a higher temperature, demonstrated greater crystallinity than its H^+ counterpart and was therefore more suitable for crystallographic analysis. Table VI shows the powder XRD data for $Na_{0.8}Ti_3O_{6.4}$.

The new structure closely resembles that of TiO_2 (B) in both relative intensities and positions of the diffraction peaks. Attempts to fit the data to a cell similar to that of TiO_2 (B) were unsuccessful; however, some useful crystallographic information was gained. All of the titanate structures—layered, condensed, and TiO_2 (B)—have in common a strong (020) reflection at $d \approx 1.87$ Å, and the new material shows a strong peak at 1.873 Å which can be given the Miller index (020). Assigning an index of (200) to the 6.9Å peak implies that the (110) should be observed at $d = 3.61$ Å. There is a strong peak at 3.61 Å, and indexing it as (110) is consistent with the other titanates, which also show strong (110) reflections. Additionally, a medium intensity peak at 2.912 Å corresponds closely to the (310) reflection ($d = 2.905$ Å) calculated using this indexing scheme. Therefore, it seems logical to conclude that the (200) and (020) peaks have been assigned correct d spacings. Unfortunately, c and β could not be deduced from the XRD data. Trial indexing schemes using the proposed (200) and (020) reflections failed to yield lattice parameters that accounted for all the diffraction peaks.

TABLE VI

POWDER X-RAY DIFFRACTION DATA FOR $Na_{0.8}H_{1.2}Ti_3O_7$ HEATED TO 800°C IN AIR

d_{obs} (Å)	I_{obs}
6.90	47
6.38	49
3.62	100
3.52	33 (anatase)
3.022	62
2.949	50
2.912	35
2.761	42
2.461	9
2.088	50
2.040	51
1.873	76
1.736	17
1.614	21
1.591	10
1.548	10

Therefore, electron diffraction was used in order to correlate the powder data with the additional information available by single crystal diffraction. Figure 16 shows an [001] zone axis diffraction pattern of the unknown structure. Using the first higher order Laue zone yields an approximate spacing for the (001) plane of 22 Å (±2 Å). A long (>20 Å) c axis yields several unit cells which are consistent with the X-ray diffraction data, and the long axis is also consistent with the observation of weak reflections in electron diffraction-corresponding lattice spacings greater than the largest spacing observed by XRD.

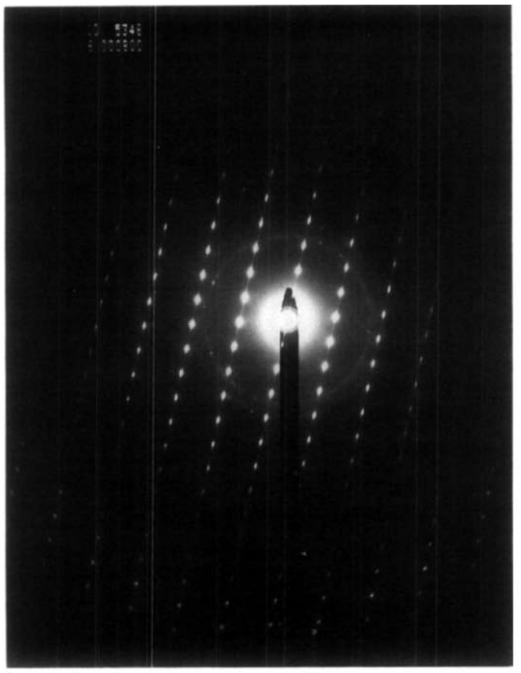

FIG. 16. [001] zone axis electron diffraction pattern of $Na_{0.8}H_{1.2}Ti_3O_7$ heated to 800°C in air.

Electron diffraction also shows several other interesting phenomena. Figure 17 shows diffraction patterns comprising the [110] zone and a zone that contains the 3.02-Å spacing observed by XRD. The patterns show streaking along the latter zone and superlattice reflections corresponding to tripling and quadrupling of the primary (3.02 Å) spacing. The supercell reflections may be due to ordering of titanium vacancies or Na ions. The streaking in these patterns, as well as along the [200] direction (Fig. 16), indicates that there is significant disorder within the structure. These observations are consistent with the metastable nature of the material. Also worth noting are the unusual intensity variations in the supercell reflections (Fig. 17a). Looking along the lines of extra reflections parallel to the [110] direction, one can see a shift of intensity from one line of extra reflections to the next across the center of the pattern. This phenomenon was reproducible, but at present we can offer no explanation for this behavior.

The data presented above point to the conclusion that the intermediate structure is closely related to TiO_2 (B) and likely contains intergrowths of another titanium oxide structure. Bando, *et al.* (*20–22*) have described several structures, with the formula $Na_2Ti_9O_{19}$, that contain blocks of TiO_2 (B) connected by bridging layers of TiO_6 octahedra and sodium ions (Fig. 18). The ratio of Na to Ti is 2 : 9, slightly more than that of the intermediate (2 : 10), and the calculated XRD patterns of the monoclinic and orthorhombic modifications of this material, though similar to TiO_2 (B), do not match that of the intermediate structure. The existence of these materials which are closely related to TiO_2 (B) does, however, lend strength to the argument that the final intermediate can possess a complicated structure composed of building blocks that resemble TiO_2 (B).

X-ray diffraction shows that the same TiO_2 (B)-like intermediate structure also forms upon dehydration of acid-exchanged $K_2Ti_4O_9$ and $Cs_2Ti_5O_{11}$ between 250 and 350°C. This indicates that its formation is not dependent on the specific structure of the starting layered titanate. The Raman spectrum of the exchanged step 5 material heated to 220° resembles that of TiO_2 (B), showing broad, poorly resolved peaks in the same positions as those of TiO_2 (B). The similarity of these two vibrational spectra emphasizes the close relationship between the structure and the bonding of the Ti–O framework in the intermediate and in TiO_2 (B).

TiO_2 (B) forms in a single step from the final intermediate, with a loss of ~0.25 mole of H_2O (i.e., $H_{0.5}Ti_3O_{6.25} \rightarrow Ti_3O_6$). The transformation occurs at temperatures as low as 280°C when samples are heated for more than 1 month, but TiO_2 (B) prepared

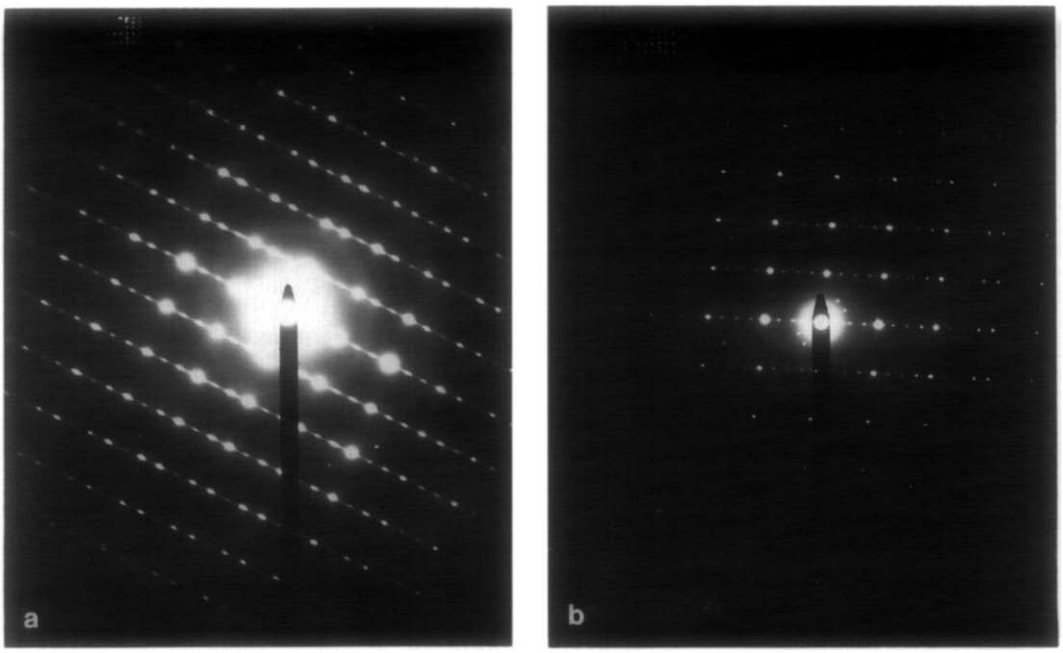

FIG. 17. Electron diffraction patterns of $Na_{0.8}H_{1.2}Ti_3O_7$ heated to 800°C in air showing (a) tripling and (b) quadrupling of the 3.02-Å lattice spacing.

at temperatures below 500°C is generally poorly crystalline and contains residual protons. Heating at temperatures of 500–700°C for short periods (1–2 hr) produces more crystalline samples, but prolonged heating at temperatures above 550° results in the slow transformation of TiO_2 (B) to anatase, as described by Brohan *et al.* (*23*).

The results presented here, which indicate that the first step of TiO_2 (B) formation involves a simple condensation of the initial layered structure to a tunnel structure, conflict with the data and conclusions of the original work on $K_2Ti_4O_9$ (*10, 13*). Those workers observed multistep dehydration, but concluded that the steps corresponded to loss of the intercalated water molecule in $H_2Ti_4O_9 \cdot H_2O$ according to the reaction

$$H_2Ti_4O_9 \cdot H_2O \rightarrow H_2Ti_4O_9 \cdot 0.5H_2O \rightarrow H_2Ti_4O_9.$$

They proposed that $H_2Ti_4O_9$ then loses 1 mole of water in a single step to form TiO_2 (B). This reaction scheme is not consistent with the mechanism of TiO_2 (B) formation proposed above; therefore we performed TGA experiments identical to the ones reported originally for acid-exchanged $K_2Ti_4O_9$. As Fig. 6 shows, the first mole of water is lost from $H_2Ti_4O_9 \cdot H_2O$ in a single step to form $H_2Ti_4O_9$, and several distinct steps follow during the formation of TiO_2 (B). Intermediate structures between the layered titanate $H_2Ti_4O_9$ and TiO_2 (B) could indeed be isolated and characterized.

The information gained from the DSC experiments further elucidates the mechanism of the transformation of layered titanates to TiO_2 (B). Calorimetric measurements, like TGA, demonstrate several distinct transitions during the dehydration of each of the layered titanates, with the number and complexity of transitions increasing with the increasing step length of the starting titanate.

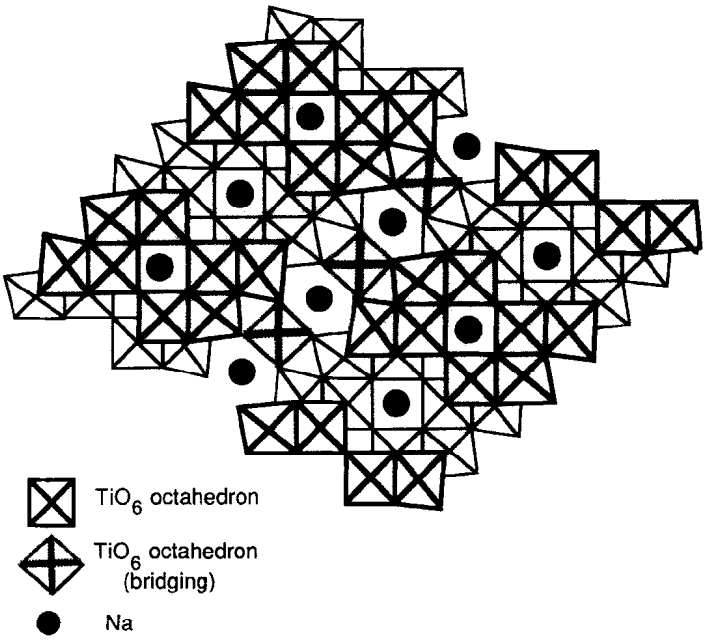

FIG. 18. The structure of $Na_2Ti_9O_{19}$.

First, let us consider the formation of TiO_2 (B) from the step 3 materials $H_2Ti_3O_7$ and $H_2Ti_6O_{13}$.

A simple condensation of the layered structure $H_2Ti_3O_7$ into a tunnel structure would be expected to show a strong endothermic heat effect. Because no major structural rearrangement occurs there is not a large energy gain from formation of a more stable crystal lattice. Therefore the bulk of the heat effect would be expected to reflect the energy necessary to drive H_2O out of the structure. $H_2Ti_3O_7$ shows exactly such an endotherm at 250°C (Fig. 10). The peak is sharp and correlates well with the TGA data. ΔH for the transformation is 47.54 J/g · degree. $H_2Ti_6O_{13}$, on the other hand, does not show an analogous transition (Fig. 13) because the structure is already condensed.

In contrast to the condensation step, major structural rearrangement to form the second intermediate would be expected to show a much different heat effect. The transformation of the step 3 titanate to the second intermediate, which likely contains the double octahedral ribbons of TiO_2 (B), might be expected to form by a reconstructive nucleation and growth mechanism. That is, the new crystal structure would nucleate at some point on or within a grain of the condensed structure and proceed to grow through the grain. The energetics for this type of structural rearrangement would be strongly exothermic, with the bulk of the heat effect reflecting the energy gain from formation of a new, more stable crystal lattice. Both $H_2Ti_3O_7$ and $H_2Ti_6O_{13}$ show a strong exothermic peak between 300 and 400°C that corresponds to the formation of the final intermediate structure. ΔH of this transition is -39.82 J/g · degree for $H_2Ti_3O_7$ and -39.20 J/g · degree for $H_2Ti_6O_{13}$. The nearly identical values demonstrate that the intermediate is forming from a condensed step 3 structure in each case.

The final transition to TiO_2 (B) from a structurally similar intermediate would be expected to be of rather low energy, because it involves little water loss and minimal rearrangement of the Ti–O framework. The DSC data for both the layered and the condensed step 3 structures show little variation of c_p as a function of temperature, confirming the low-energy nature of this transition.

Acid-exchanged $K_2Ti_4O_9$ and $Cs_2Ti_5O_{11}$ behave similarly to the step 3 materials, with the exception that both show large endothermic peaks at approximately 100°C, corresponding to topotactic water loss. ΔH of this transition for $H_2Ti_5O_{11} \cdot 2.5H_2O \rightarrow H_2Ti_5O_{11}$ is 251.9 J/g · degree, and for $H_2Ti_4O_9 \cdot H_2O \rightarrow H_2Ti_4O_9$ the value is 67.6 J/g · degree. The second transition for each material is endothermic, but more poorly defined than that of the step 3 materials. This correlates well with the XRD data that show it is difficult to isolate a single-phase, crystalline intermediate structure after this step. The following transition is exothermic and leads to the formation of the same TiO_2 (B)-like intermediate structure as discussed above. The transition is broadest for the step 5 titanate, implying that there is not as strong a driving force for formation of the intermediate from titanates with a longer starting step length. This is consistent with the XRD and Raman results, which show that the TiO_2 (B) formed at the end of the dehydration reaction is less crystalline for longer step length starting structures.

Exchanged $K_2Ti_4O_9$ shows a large exotherm at approximately 520°C which results not from TiO_2 (B) formation, which occurs by 500°C, but from the formation of anatase. TGA showed an anomalous weight loss for this sample at 520°C, and X-ray diffraction indicates that the appearance of additional anatase is the only result of this step. The total weight loss before this step corresponds to the loss of 2 mole of water from $H_2Ti_4O_9 \cdot H_2O$ to form $4TiO_2$ ((B) + anatase). The further anatase formation likely results from crystallization of an amorphous, hydrated precursor, the product of decomposition of the layered structure over time. DSC data for the other titanate samples, which were collected soon after sample preparation, do not show the exothermic transition or final weight loss step.

TABLE VII

COMPARISON OF REFINED ATOMIC COORDINATES OF TiO_2 (B) WITH THOSE PREDICTED BY THE ENERGY MINIMIZATION TECHNIQUE

	This work			Catlow *et al.* (*18*)[a]		
Atom	*x*	*y*	*z*	*x*	*y*	*z*
Ti(1)	0.197	0	0.292	0.184	0	0.278
Ti(2)	0.099	0	0.705	0.097	0	0.736
O(1)	0.132	0	0.004	0.127	0	0.009
O(2)	0.264	0	0.653	0.264	0	0.658
O(3)	0.060	0	0.371	0.057	0	0.369
O(4)	0.362	0	0.293	0.354	0	0.277

[a] The values reported in this column were obtained by transforming the reported values by $(-x, -y, -z)$.

TABLE VIII

INTERATOMIC DISTANCES (Å) FOR Ti–O (B)

Ti(1)		O(1)	
–Ti(1)	3.236(8)	–O(1)	3.196(1)
–Ti(2)	3.252(1)	–O(1)	3.447(1)
–Ti(2)	3.107(9)	–O(2)	3.158(1)
–O(1)	1.812(1)	–O(2)	2.906(12)
–O(2)	2.257(1)	–O(3)	2.777(1)
–O(2) (2x)	1.938(5)	–O(3)	2.846(19)
–O(3)	1.883(1)	–O(4)	2.876(1)
–O(4)	1.997(1)	–O(4)	2.716(1)
Ti(2)		O(2)	
–Ti(2)	3.030(15)	–O(2)	2.687(1)
–O(1)	1.874(1)	–O(3)	2.619(1)
–O(2)	2.130(1)	–O(3)	2.887(7)
–O(3)	2.091(1)	–O(4)	2.926(1)
–O(3)	1.852(16)	–O(4)	2.498(2)
–O(4) (2x)	1.932(3)		
		–O(3)	2.535(1)
		–O(4)	2.984(1)
		–O(4)	2.826(10)

Note. The estimated standard deviations are in 0.001 Å.

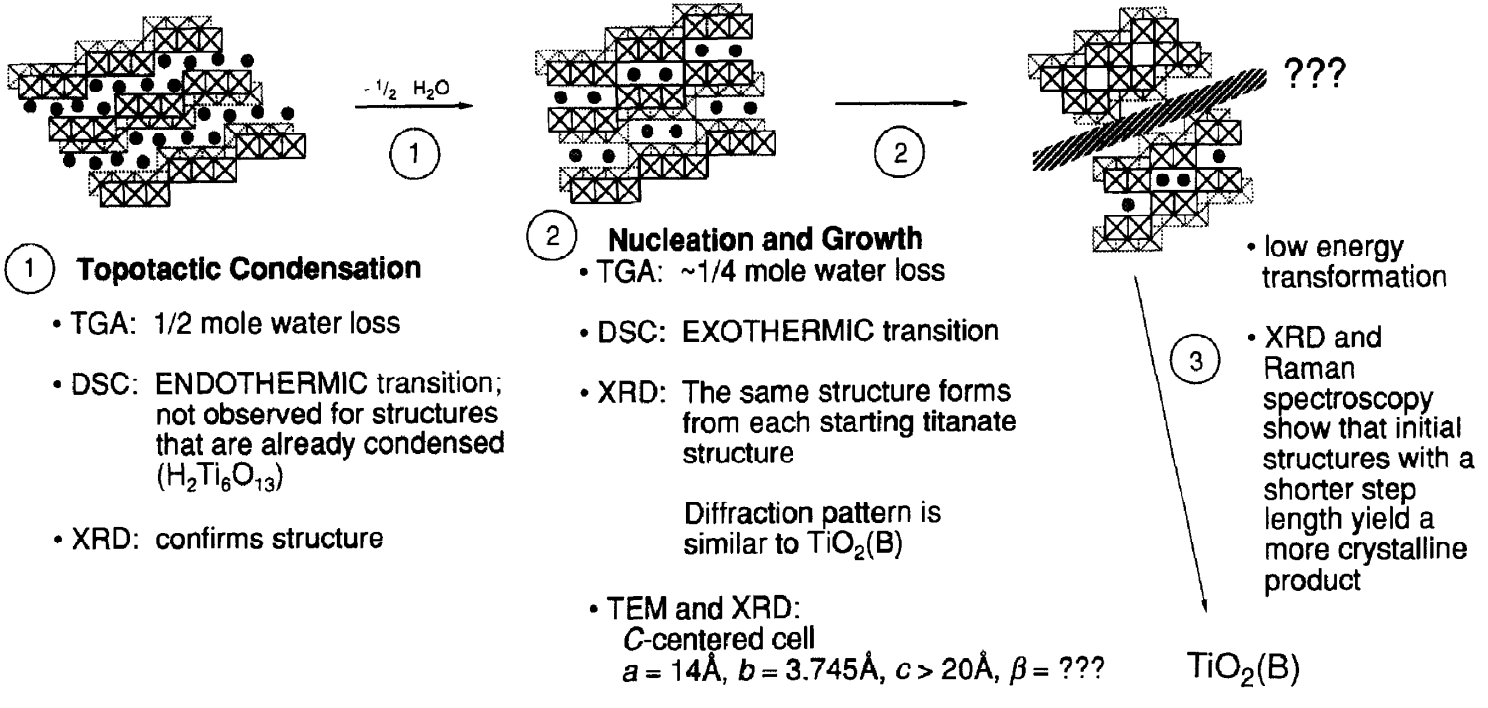

FIG. 19. Mechanistics of the formation of TiO_2 (B) from $H_2Ti_3O_7$.

The atomic parameters of TiO_2 (B) refined from neutron diffraction data collected at room temperature compare well with those predicted by Catlow *et al.* (*18*) using the energy minimization technique (Table VII). The refinement showed no indication of partial site occupancy for titanium or oxygen, so the occupancies of these atoms were fixed at 1. The Fourier difference map showed no evidence for residual Na in the structure, and attempts to include it did not improve the *R* value for the refinement. Table VIII shows the final interatomic distances obtained from Rietveld refinement of the TiO_2 (B) structure. The distances are consistent with those observed for other Ti–O octahedral framework structures. The experiment confirms that TiO_2 (B) is a metastable form of pure TiO_2, and it does not result from stabilization of the structure by residual alkali metal cations.

Conclusion

A variety of layered titanates undergo ion-exchange reactions, and subsequent dehydration of the exchanged materials results in the formation of TiO_2 (B). The acid-exchanged titanates have an ABA stacking sequence of layers which results from the formation of stable hydrogen bonds between the layers. The oxygens bonded to only one titanium are the most basic and therefore most strongly protonated. Upon heating, the materials demonstrate multistep weight loss behavior, with the appearance of distinct structural intermediates. Figure 19 shows a schematic representation of the stages in the transformation of $H_2Ti_3O_7$ to TiO_2 (B). The first step is a condensation of the layers, in which the hydrogen bonds are disrupted as the layers join together through corner-sharing TiO_6 octahedra. This simple topotactic condensation of the layered material into a tunnel structure, which is an endothermic reaction, appears to be common to each of the layered titanates. The succeeding step, characterized by an exothermic heat effect, is a nucleation and growth reaction in which each of the materials studied forms a TiO_2 (B)-like intermediate. The intermediate structure appears to consist of TiO_2 (B)-like slabs connected by other structural units capable of tolerating some Ti and/or O nonstoichiometry. Upon complete dehydration, each of the titanates forms TiO_2 (B) from the final intermediate in a single step, and the crystallinity of the TiO_2 (B) is strongly dependent on the step length of the starting material and the dehydration temperature.

Acknowledgments

The authors gratefully acknowledge the support of the National Science Foundation (DMR-88-19027), Exxon Research and Engineering Corp., and IBM Corp. We also acknowledge the National Science Foundation, MRL program (Grant DMR-88-19885), for support of the electron microscopy facility. We especially thank Dr. A. J. Jacobson for his many valuable suggestions and discussions. B. M. Powell (AECL), J. E. Fischer, and J. M. Newsam provided much assistance in the collection and interpretation of neutron diffraction data, and the help of F. Hardcastle and R. B. Hall in collecting Raman spectroscopy data is also acknowledged.

References

1. R. Marchand, L. Brohan, and M. Tournoux, *Mater. Res. Bull.* **15,** 1129 (1980).
2. S. J. Mocarski, Master's thesis, University of Pennsylvania (1986).
3. T. P. Feist, S. J. Mocarski, P. K. Davies, A. J. Jacobson, and J. T. Lewandowski, *Solid State Ionics,* **28–30,** 1338 (1988).
4. M. Dion, Y. Piffard, and M. Tournoux, *J. Inorg. Nucl. Chem.* **40,** 917 (1978).
5. F. Théobald, R. Cabala, and J. Bernard, *J. Solid State Chem.* **17,** 431 (1976).
6. S. Andersson and A. D. Wadsley, *Acta Crystallogr.* **15,** 201 (1962).
7. J. Papachryssanthou, E. Bordes, A. Vejux, P. Coutine, R. Marchand, and M. Tournoux, *Catal. Today* **1,** 219 (1987).
8. L. Brohan and R. Marchand, *Solid State Ionics* **9/10,** 419 (1983).
9. G. Betz, H. Tributsch, and R. Marchand, *J. Appl. Electrochem.* **14,** 315 (1984).

10. R. MARCHAND, L. BROHAN, R. M'BEDI, AND M. TOURNOUX, *Rev. Chim. Miner.* **21,** 476 (1984).
11. L. BROHAN, R. MARCHAND, AND M. TOURNOUX, *Mater. Sci. Monogr. 25A (10th Int. Conf. React. Solids)*, 481 (1985).
12. M. TOURNOUX, *Inform. Chim.* (239), 69 (1983).
13. M. TOURNOUX, R. MARCHAND, AND L. BROHAN, Prog. Solid State Chem. **17,** 33 (1986).
14. H. IZAWA, S. KIKKAWA, AND H. KOIZUMI, *J. Phys. Chem.* **86,** 5023 (1982).
15. S. ANDERSSON AND A. D. WADSLEY, *Acta Crystallogr.* **14,** 1245 (1961).
16. S. ANDERSSON AND A. D. WADSLEY, *Acta Crystallogr.* **15,** 194 (1962).
17. I. E. GREY, I. C. MADSEN, J. A. WATTS, L. A. BURSILL, AND J. KWIATKOWSKA, *J. Solid State Chem.* **58,** 350 (1985).
18. C. R. A. CATLOW, A. CORMACK, AND F. THÉOBALD, *Acta Crystallogr. B* **40,** 195 (1984).
19. H. REBBAH, J. PANNETIER, AND B. RAVEAU, *J. Solid State Chem.* **41,** 57 (1982).
20. Y. BANDO, M. WATANABE, AND Y. SEKIKAWA, *Acta Crystallogr. B* **35,** 1541 (1979).
21. Y. BANDO, M. WATANABE, AND Y. SEKIKAWA, *J. Solid State Chem.* **33,** 413 (1980).
22. M. WATANABE, Y. BANDO, AND M. TSUTSUMI, *J. Solid State Chem.* **28,** 397 (1979).
23. L. BROHAN, A. VERBAERE, AND M. TOURNOUX, *Mater. Res. Bull.* **17,** 355 (1982).